

Coarsening dynamics driven by vortex-antivortex annihilation in ferromagnetic Bose-Einstein condensates

Kazue Kudo¹ and Yuki Kawaguchi²

¹*Department of Computer Science, Ochanomizu University,
2-1-1 Ohtsuka, Bunkyo-ku, Tokyo 112-8610, Japan*

²*Department of Applied Physics, University of Tokyo,
7-3-1 Hongo, Bunkyo-ku, Tokyo 113-8656, Japan*

(Dated: February 27, 2018)

In ferromagnetic Bose-Einstein condensates (BECs), the quadratic Zeeman effect controls magnetic anisotropy, which affects magnetic domain pattern formation. While the longitudinal magnetization is dominant (similar to the Ising model) for a negative quadratic Zeeman energy, the transverse magnetization is dominant (similar to the XY model) for a positive one. When the quadratic Zeeman energy is positive, the coarsening dynamics is driven by vortex-antivortex annihilation in the same way as the XY model. However, due to superfluid flow of atoms, there exist several combinations of vortex-antivortex pairs in ferromagnetic BECs, which makes the coarsening dynamics more complicated than that of the XY model. We propose a revised domain growth law, which is based on the growth law of the two-dimensional XY model, for a two-dimensional ferromagnetic BEC with a positive quadratic Zeeman energy.

PACS numbers: 03.75.Lm, 89.75.Kd, 03.75.Kk, 03.75.Mn

I. INTRODUCTION

Domain growth and coarsening dynamics have been studied in a wide variety of systems [1–11]. When a system is quenched from a disordered phase to an ordered phase, the long-range order does not arise immediately. At first, locally-ordered small domains arise, which then grow with time to make global order through domain coarsening. Although there are different mechanisms to cause domain growth, in most cases, domain size l grows with time t as $l(t) \sim t^\nu$, where ν is a scaling exponent. For example, $\nu = 1/3$ in the two-dimensional (2D) conserved systems described by the Ising model (e.g., binary alloys and ferromagnets with uniaxial anisotropy) [1–4]. If fluid flow contributes to domain growth, which is the case of binary fluids, the exponent changes depending on advection and viscosity. When the advective transport is negligible, diffusion dominates the coarsening dynamics. In that case, $\nu = 1/3$ [5], which is the same as in the absence of flow. However, if the advective transport with little viscosity dominates over diffusion, the inertia of fluid becomes important in the coarsening dynamics. In this case, domains grow faster than the diffusive case, and the exponent is $\nu = 2/3$ [6]. When the system is described by vector fields (i.e., complex order parameters or multi-component order parameters), the dominant mechanism to cause domain growth is completely different from those for the Ising model and binary fluids. For example, the coarsening dynamics for 2D vector fields is driven by the annihilation of vortex-antivortex pairs. The domain size, which is actually the characteristic length of the spatial structure of the field, grows as $l(t) \sim t^{1/2}$ for non-conserved n -component vector fields in d -dimensional space, except for $d = n = 2$, namely, the 2D XY model. The domain growth law for the 2D XY model includes a logarithmic correction:

$$l(t) \sim (t/\ln t)^{1/2} \text{ [7–11].}$$

Magnetic domain patterns and their coarsening dynamics are observed also in ferromagnetic Bose-Einstein condensates (BECs). Recent development in imaging techniques to observe magnetization profiles in ferromagnetic BECs has enabled us to investigate the real-time dynamics of magnetization, such as spin texture formation, spin-domain coarsening, and nucleation of spin vortices [12–15]. Those experiments have also motivated theoretical studies about configurations of Skyrmions and spin textures [16, 17], magnetic domain formation [18, 19], and spin turbulence [20–22]. Magnetic anisotropy of a ferromagnetic BEC depends on the quadratic Zeeman energy, which can be controlled by external fields. When the quadratic Zeeman energy is negative, longitudinal magnetization is dominant, and thus the system is similar to the Ising model. In 2D ferromagnetic BECs with a negative quadratic Zeeman energy or binary BECs, domain size grows as $l(t) \sim t^{2/3}$ [19, 23], which has the same exponent $\nu = 2/3$ as that for binary fluids in the inertial hydrodynamic regime. However, $l(t) \sim t^{1/3}$ in the absence of superfluid flow [19]. The difference in the exponents suggests that the superfluid flow has a strong influence on the coarsening dynamics.

In this paper, we investigate the coarsening dynamics in 2D spin-1 ferromagnetic BECs with a positive quadratic Zeeman energy. When the quadratic Zeeman energy is positive, transverse magnetization is dominant, and the coarsening dynamics is caused by vortex-antivortex annihilation. The situation is similar to the 2D XY model, however a crucial difference arises in the classification of vortices. Vortices in ferromagnetic BECs are classified by the winding number of spin current (direction of magnetization) and mass current (vorticity of superfluid flow). Thus, there are several combinations of vortex-antivortex pairs which cause pair annihilation

in ferromagnetic BECs. By contrast, in the XY model, there is only one combination of vortex-antivortex pairs. When several combinations of annihilation pairs exist, the coarsening dynamics is expected to be more complicated than that of the XY model. In other words, superfluid flow has indirect effects on the coarsening dynamics through different combinations of vortex-antivortex annihilation. We will demonstrate the coarsening dynamics in ferromagnetic BECs by numerical simulations, and propose a revised domain growth law, based on the growth law for the XY model.

The rest of the paper is organized as follows. The decay of the vortex density, which is caused by vortex-antivortex annihilation, in ferromagnetic BECs is discussed in Sec. II. Numerical simulations illustrated in Sec. III clearly show that superfluid flow affects the coarsening dynamics and that a revised growth law is needed for the case where there are several combinations of vortex-antivortex pairs. The revised law is proposed in Sec. IV. Discussions and conclusions are given in Sec. V.

II. DOMAIN GROWTH LAW

A. Interaction of vortices

We consider a spin-1 BEC confined in the x - y plane under a uniform magnetic field applied in the z direction. For simplicity, we neglect the confining potential in the x and y directions. The mean-field kinetic energy and Zeeman energy are given by

$$E_{\text{kin}} = \int d\mathbf{r} \sum_{m=-1}^1 \Psi_m^*(\mathbf{r}) \left(-\frac{\hbar^2}{2M} \nabla^2 \right) \Psi_m(\mathbf{r}), \quad (1)$$

$$E_q = \int d\mathbf{r} \sum_{m=-1}^1 qm^2 |\Psi_m(\mathbf{r})|^2, \quad (2)$$

where $\Psi_m(\mathbf{r})$ is the condensate wave function for the atoms in the magnetic sublevel m , M is an atomic mass, and q is the quadratic Zeeman energy per atom. Here, we neglected the linear Zeeman term because the linear Zeeman effect merely induces the Larmor precession of atomic spins and can be eliminated in the rotating frame of reference. The quadratic Zeeman energy is tunable by means of a linearly polarized microwave field and can take both positive and negative values [24, 25].

The interatomic interaction energy is given by

$$E_{\text{int}} = \frac{1}{2} \int d\mathbf{r} [c_0 n_{\text{tot}}(\mathbf{r})^2 + c_1 |\mathbf{f}(\mathbf{r})|^2], \quad (3)$$

where the number density and the spin density (local

magnetization) are given by

$$n_{\text{tot}}(\mathbf{r}) = \sum_{m=-1}^1 |\Psi_m(\mathbf{r})|^2, \quad (4)$$

$$f_\nu(\mathbf{r}) = \sum_{m,n=-1}^1 \Psi_m^*(\mathbf{r}) (F_\nu)_{mn} \Psi_n(\mathbf{r}), \quad (5)$$

respectively. Here, $\nu = x, y, z$ and, $F_{x,y,z}$ are the spin-1 matrices. The interaction coefficients are given by $c_0 = 4\pi\hbar^2(2a_2 + a_0)/(3M)$ and $c_1 = 4\pi\hbar^2(a_2 - a_0)/(3M)$, where a_s is the s -wave scattering lengths of two colliding atoms with total spin S channel. For the condensate to be stable, c_0 needs to be positive. On the other hand, the sign of c_1 determines the magnetism: the condensate is ferromagnetic (antiferromagnetic or polar) for $c_1 < 0$ ($c_1 > 0$). In this paper, we consider ferromagnetic BECs ($c_1 < 0$).

When the quadratic Zeeman energy is weak compared with the ferromagnetic interaction energy, the condensate is fully magnetized ($|\mathbf{f}| = n_{\text{tot}}$). Since the order parameter for a fully-magnetized state in the direction $(\cos \alpha \sin \beta, \sin \alpha \sin \beta, \cos \beta)$ is given by [26, 27]

$$\Psi \equiv \begin{pmatrix} \Psi_1 \\ \Psi_0 \\ \Psi_{-1} \end{pmatrix} = \sqrt{n_{\text{tot}}} e^{i\phi} \begin{pmatrix} e^{-i\alpha} \cos^2 \frac{\beta}{2} \\ \sqrt{2} \sin \frac{\beta}{2} \cos \frac{\beta}{2} \\ e^{i\alpha} \sin^2 \frac{\beta}{2} \end{pmatrix}, \quad (6)$$

the population in the $m = 0$ component becomes maximum at $\beta = \pi/2$, whereas those in the $m = 1$ and -1 components become maximum at $\beta = 0$ and π , respectively. As seen from Eq. (2), the quadratic Zeeman effect enhances the population in the $m = 0$ state for $q > 0$ and those in the $m = \pm 1$ states for $q < 0$. Hence, the magnetization arises in the x - y plane ($\beta = \pi/2$) for $q > 0$, and in the $+z$ or $-z$ direction ($\beta = 0$ or π) for $q < 0$. The former case corresponds to the XY model and the latter the Ising model of the conventional ferromagnet. Although the magnitude of the spontaneous magnetization becomes smaller when the quadratic Zeeman energy is positive and comparable to the ferromagnetic interaction, the magnetization direction is still confined in the x - y plane. Since we are interested in vortex-antivortex annihilation, we consider $q > 0$ below.

We first consider a single vortex and write its wave function in the polar coordinate whose origin is the center of the vortex core: $\Psi(r, \varphi)$. We take $\phi = \sigma_\phi \varphi$ and $\alpha = \sigma_\alpha \varphi$ in Eq. (6), where σ_ϕ and σ_α are integers. For a symmetric vortex, β is a function of r and independent of φ . At a distance from the vortex core, $\beta = \pi/2$ as discussed in the above. The wave function outside of the core is approximately written as

$$\Psi = \frac{\sqrt{n_{\text{tot}}}}{2} e^{i\sigma_\phi \varphi} \begin{pmatrix} e^{-i\sigma_\alpha \varphi} \\ \sqrt{2} \\ e^{i\sigma_\alpha \varphi} \end{pmatrix}. \quad (7)$$

Here, σ_ϕ and σ_α determine the directions of mass flow and spin flow around the vortex, respectively. The superfluid velocity (mass flow) and the spin superfluid velocity

(spin flow) of z component are written for a homogeneous n_{tot} as

$$\mathbf{v}_{\text{mass}} = \frac{\hbar}{2Mi} \sum_{m=-1}^1 [\Psi_m^* (\nabla \Psi_m) - (\nabla \Psi_m^*) \Psi_m] / n_{\text{tot}}, \quad (8)$$

$$\mathbf{v}_{\text{spin}}^z = \frac{\hbar}{2Mi} \sum_{m=-1}^1 (F_z)_{mn} [\Psi_m^* (\nabla \Psi_n) - (\nabla \Psi_m^*) \Psi_n] / n_{\text{tot}}, \quad (9)$$

respectively. Substituting Eq. (7) into Eqs. (8) and (9), we see that the directions of mass and spin flows depend on σ_ϕ and σ_α , respectively, as $\mathbf{v}_{\text{mass}} = \sigma_\phi (\hbar/M) \nabla \varphi$ and $\mathbf{v}_{\text{spin}}^z = -\sigma_\alpha (\hbar/2M) \nabla \varphi$.

The combination of σ_ϕ and σ_α also determines the vortex core structure. Though we use $\beta = \pi/2$ in Eq. (7), β changes around the center of the vortex so as to remove the singularity of the order parameter. When $\sigma_\phi = \sigma_\alpha$, the $m = 1$ component is independent of φ and only this component remains at $r = 0$. In this case, β takes 0 at $r = 0$, which means the magnetization at the center is in the $+z$ direction for $\sigma_\phi = \sigma_\alpha$. Similarly, for vortices with $\sigma_\phi = -\sigma_\alpha$, magnetization is in the $-z$ direction at the center. When $\sigma_\phi = 0$ and $\sigma_\alpha \neq 0$, φ -dependent components cannot vanish in a fully-magnetized state. Thus, magnetization vanishes at the center for $\sigma_\phi = 0$. On the other hand, when $\sigma_\phi \neq 0$ and $\sigma_\alpha = 0$, all three components should vanish at the center. In the following, we consider only the elementary vortices that are stable against splitting, that is, $\sigma_\phi = 0, \pm 1$ and $\sigma_\alpha = \pm 1$. The vortex of $\sigma_\phi = 0$ has no mass flow around itself and its core is not magnetized. Such a vortex is called polar-core vortex (PCV). When $\sigma_\phi = \pm 1$, the vortex has mass flow around its core and its core is fully magnetized as well as the outside. Such a vortex is called Mermin-Ho vortex (MHV). Considering the combination of σ_ϕ and σ_α , we notice that there are two kinds of PCVs $[(\sigma_\phi, \sigma_\alpha) = (0, \pm 1)]$ and four kinds of MHVs $[(\sigma_\phi, \sigma_\alpha) = (\pm 1, \pm 1)]$.

A vortex-antivortex pair is defined so that they can be pair-annihilated. For the case of a single-component BEC, two vortices with winding numbers with the opposite signs are a vortex-antivortex pair. In the present case, i.e., a multi-component BEC, when two vortices have winding numbers with the opposite signs in all components, they can be annihilated as a vortex-antivortex pair. For the vortex expressed by Eq. (7), the $m = 1, 0$, and -1 components have the winding numbers $\sigma_\phi - \sigma_\alpha$, σ_ϕ , and $\sigma_\phi + \sigma_\alpha$, respectively. Thus, its antivortex is obtained by changing the signs of both σ_ϕ and σ_α . In other words, vortices with $(\sigma_\phi, \sigma_\alpha)$ and $(-\sigma_\phi, -\sigma_\alpha)$ are a vortex-antivortex pair.

In this paper, we consider only MHVs, which are useful to investigate the effect of superfluid flow. Using Eq. (7),

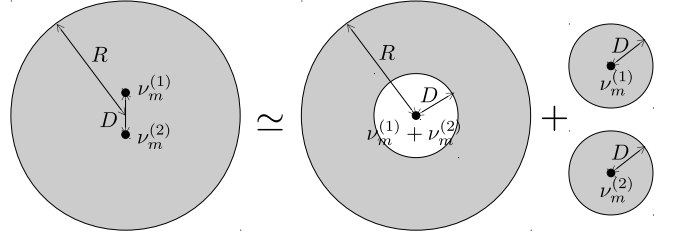


FIG. 1. Evaluation of the energy E_{pair} of two vortices with vorticities $\nu_m^{(1)}$ and $\nu_m^{(2)}$ separated by a distance D .

we estimate the kinetic energy of a single vortex as

$$\begin{aligned} E_s &= \frac{\hbar^2}{2M} \int d^2r \sum_m (\nabla \Psi_m^*) \cdot (\nabla \Psi_m) \\ &\simeq \frac{\hbar^2}{2M} \int_{R_c}^R r dr \int_0^{2\pi} d\varphi \sum_m (\nabla \Psi_m^*) \cdot (\nabla \Psi_m) \\ &= C \mathcal{N}_1 \log \left(\frac{R}{R_c} \right), \end{aligned} \quad (10)$$

where $C = \pi \hbar^2 n_{\text{tot}} / M$, and R and R_c are the vortex size (radius) and the radius of the vortex core, respectively. Although R is equal to the system size for a single vortex, it is the distance beyond which the field around the vortex is shielded if there are other vortices. \mathcal{N}_1 depends on σ_ϕ and σ_α . Since the portions of the number densities for $m = 1, 0, -1$ are $\frac{1}{4}, \frac{1}{2}, \frac{1}{4}$, respectively,

$$\mathcal{N}_1 = \frac{\nu_1^2}{4} + \frac{\nu_0^2}{2} + \frac{\nu_{-1}^2}{4}, \quad (11)$$

where $\nu_1 = \sigma_\phi - \sigma_\alpha$, $\nu_0 = \sigma_\phi$, and $\nu_{-1} = \sigma_\phi + \sigma_\alpha$.

The interaction energy between two vortices at a distance of D is given by $V(D) = E_{\text{pair}}(D) - E_1 - E_2$, where E_{pair} is the energy of two vortices separated by a distance D , E_1 and E_2 are the energies of single vortices with vorticities $\nu_m^{(1)}$ and $\nu_m^{(2)}$, respectively. The pair energy E_{pair} is approximately given by the sum of contributions from two regions (see Fig. 1). In the region of $D < r < R$, the contribution is evaluated for a single (composite) vortex with vorticity $\nu_m^{(1)} + \nu_m^{(2)}$. In the region of $r < D$, the contribution is just the sum of E_1 and E_2 . Then, the interaction energy is approximated by

$$V(D) = C \mathcal{N}_2 \log \left(\frac{R}{D} \right), \quad (12)$$

$$\mathcal{N}_2 = \frac{\nu_1^{(1)} \nu_1^{(2)}}{2} + \nu_0^{(1)} \nu_0^{(2)} + \frac{\nu_{-1}^{(1)} \nu_{-1}^{(2)}}{2}. \quad (13)$$

The derivative of $V(D)$ gives the force between the vortex pair,

$$F_{\text{pair}} = -\frac{dV(D)}{dD} = \frac{C \mathcal{N}_2}{D}, \quad (14)$$

which is an attractive force between a vortex-antivortex pair. Note that pair annihilation occurs only between a

vortex pair in which both σ_ϕ and σ_α have the opposite signs, although the force is attractive ($\mathcal{N}_2 < 0$) between vortices with the opposite signs of σ_ϕ even if they have the same sign of σ_α .

B. Coarsening dynamics

We assume that the attractive force between a vortex-antivortex pair is balanced with a friction (resistive) force F_{fric} when the pair vortices move toward each other. The friction causes energy dissipation. When a vortex moves at speed u , the energy dissipation rate is written as

$$\frac{dE}{dt} = -uF_{\text{fric}}. \quad (15)$$

The dynamics of a spinor BEC is well described with the time-dependent multi-component Gross-Pitaevskii (GP) equation, and we phenomenologically introduce an energy dissipation into the GP equation [27, 28]:

$$\begin{aligned} (i - \Gamma)\hbar\frac{\partial}{\partial t}\Psi_m(\mathbf{r}, t) \\ = \left[-\frac{\hbar^2}{2M}\nabla^2 - \mu(t) + qm^2 + c_0n_{\text{tot}}(\mathbf{r}, t) \right] \Psi_m(\mathbf{r}, t) \\ + c_1 \sum_{n=-1}^1 \sum_{\nu=x,y,z} f_\nu(\mathbf{r}, t)(F_\nu)_{mn}\Psi_n(\mathbf{r}, t), \end{aligned} \quad (16)$$

where Γ expresses energy dissipation.

In order to discuss the energy dissipation that is caused by the friction force, we employ the hydrodynamic equation, which is derived in the low-energy limit [18, 19]. In this limit, the BEC is fully magnetized, i.e., $|\mathbf{f}| = n_{\text{tot}}$, and the physical quantities that describe the dynamics of ferromagnetic BECs are the normalized spin vector

$$\hat{\mathbf{f}} \equiv \frac{\mathbf{f}}{n_{\text{tot}}}, \quad (17)$$

and the superfluid velocity \mathbf{v}_{mass} . The equations of motion for them are derived straightforwardly from the GP equation (16) [18, 19, 26], and the resulting equations of motion are written as

$$\begin{aligned} \frac{\partial \hat{\mathbf{f}}}{\partial t} = \frac{1}{1 + \Gamma^2} \left[\frac{1}{\hbar} \hat{\mathbf{f}} \times \mathbf{B}_{\text{eff}} - (\mathbf{v}_{\text{mass}} \cdot \nabla) \hat{\mathbf{f}} \right] \\ - \frac{\Gamma}{1 + \Gamma^2} \hat{\mathbf{f}} \times \left[\frac{1}{\hbar} \hat{\mathbf{f}} \times \mathbf{B}_{\text{eff}} - (\mathbf{v}_{\text{mass}} \cdot \nabla) \hat{\mathbf{f}} \right], \end{aligned} \quad (18a)$$

$$\mathbf{B}_{\text{eff}} = \frac{\hbar^2}{2M} \nabla^2 \hat{\mathbf{f}} - q\hat{f}_z \hat{\mathbf{z}}, \quad (18b)$$

$$\begin{aligned} M \frac{\partial}{\partial t} \mathbf{v}_{\text{mass}} = \frac{\hbar}{2n_{\text{tot}}\Gamma} \nabla [\nabla \cdot (n_{\text{tot}} \mathbf{v}_{\text{mass}})] \\ + \hbar (\nabla \hat{\mathbf{f}}) \cdot \left(\hat{\mathbf{f}} \times \frac{\partial \hat{\mathbf{f}}}{\partial t} \right). \end{aligned} \quad (18c)$$

Here, we assumed a uniform number density: $\nabla n_{\text{tot}} = 0$.

The kinetic energy in this formulation is written as

$$\begin{aligned} E_{\text{kin}} = \frac{\hbar^2 n_{\text{tot}}}{4M} \int d\mathbf{r} \left[(\nabla \hat{f}_x)^2 + (\nabla \hat{f}_y)^2 + (\nabla \hat{f}_z)^2 \right] \\ + \frac{M n_{\text{tot}}}{2} \int d\mathbf{r} \mathbf{v}_{\text{mass}}^2. \end{aligned} \quad (19)$$

We divide the energy dissipation into two parts, which is written as

$$\frac{dE}{dt} = \frac{dE_{\text{mag}}}{dt} + \frac{dE_{\text{flow}}}{dt}, \quad (20)$$

$$\frac{dE_{\text{mag}}}{dt} = \int d\mathbf{r} \left(\frac{\delta E}{\delta \hat{f}_x} \frac{\partial \hat{f}_x}{\partial t} + \frac{\delta E}{\delta \hat{f}_y} \frac{\partial \hat{f}_y}{\partial t} + \frac{\delta E}{\delta \hat{f}_z} \frac{\partial \hat{f}_z}{\partial t} \right), \quad (21)$$

$$\frac{dE_{\text{flow}}}{dt} = \int d\mathbf{r} \left(\frac{\delta E}{\delta v_x} \frac{\partial v_x}{\partial t} + \frac{\delta E}{\delta v_y} \frac{\partial v_y}{\partial t} \right), \quad (22)$$

where $\mathbf{v}_{\text{mass}} = (v_x, v_y)$. We assume that a vortex keeps its shape, i.e., the profiles of \mathbf{v}_{mass} and $\hat{\mathbf{f}}$ around its core, when it moves. The contribution to dE_{mag}/dt arises from the change in direction of local magnetization. Since the profiles of \mathbf{v}_{mass} and $\hat{\mathbf{f}}$ are conserved, the coupling between \mathbf{v}_{mass} and $\hat{\mathbf{f}}$ gives no contribution to dE_{mag}/dt . Neglecting the energy contributions from the vortex core, we only need to consider the hydrodynamic equation in the outside region of the vortex core. Then, Eq. (18) with $\hat{f}_z = \partial \hat{f}_z / \partial t = \nabla \hat{f}_z = 0$ leads to

$$\frac{\partial \hat{f}_x}{\partial t} = -\frac{\Gamma}{1 + \Gamma^2} \frac{\hbar}{2M} \left[\hat{f}_x (\hat{\mathbf{f}} \cdot \nabla^2 \hat{\mathbf{f}}) - \nabla^2 \hat{f}_x \right], \quad (23a)$$

$$\frac{\partial \hat{f}_y}{\partial t} = -\frac{\Gamma}{1 + \Gamma^2} \frac{\hbar}{2M} \left[\hat{f}_y (\hat{\mathbf{f}} \cdot \nabla^2 \hat{\mathbf{f}}) - \nabla^2 \hat{f}_y \right], \quad (23b)$$

$$\frac{\partial \mathbf{v}_{\text{mass}}}{\partial t} = \frac{\hbar}{2M\Gamma} \nabla (\nabla \cdot \mathbf{v}_{\text{mass}}), \quad (23c)$$

where the coupling terms with $(\mathbf{v}_{\text{mass}} \cdot \nabla) \hat{\mathbf{f}}$ are dropped. Since we take $\hat{f}_z = 0$, $\hat{f}_x = \cos \alpha$ and $\hat{f}_y = \sin \alpha$. From Eqs. (23a) and (23b), we have

$$\frac{\partial \alpha}{\partial t} = \hat{f}_x \frac{\partial \hat{f}_y}{\partial t} - \hat{f}_y \frac{\partial \hat{f}_x}{\partial t} = \frac{\Gamma}{1 + \Gamma^2} \frac{\hbar}{2M} \nabla^2 \alpha. \quad (24)$$

Substituting Eqs. (23a) and (23b) into Eq. (21) gives

$$\begin{aligned} \frac{dE_{\text{mag}}}{dt} = -\frac{\hbar^2 n_{\text{tot}}}{2M} \int d\mathbf{r} \left((\nabla^2 \hat{f}_x) \frac{\partial \hat{f}_x}{\partial t} + (\nabla^2 \hat{f}_y) \frac{\partial \hat{f}_y}{\partial t} \right) \\ = -\frac{\hbar n_{\text{tot}} (1 + \Gamma^2)}{\Gamma} \int d\mathbf{r} \left[\left(\frac{\partial \hat{f}_x}{\partial t} \right)^2 + \left(\frac{\partial \hat{f}_y}{\partial t} \right)^2 \right] \\ = -\frac{\hbar n_{\text{tot}} (1 + \Gamma^2)}{\Gamma} \int d\mathbf{r} \left(\frac{\partial \alpha}{\partial t} \right)^2, \end{aligned} \quad (25)$$

where we used $\hat{f}_x^2 + \hat{f}_y^2 = 1$. Substituting Eq. (7) into Eq. (8), we have

$$\mathbf{v}_{\text{mass}} = \frac{\hbar}{M} \nabla \phi, \quad (26)$$

where $\phi = \sigma_\phi \varphi$. Equations. (23c) and (26) lead to

$$\frac{\partial \phi}{\partial t} = \frac{\hbar}{2M\Gamma} \nabla^2 \phi. \quad (27)$$

Using Eqs. (23c), (26), and (27), we rewrite Eq. (22) as

$$\begin{aligned} \frac{dE_{\text{flow}}}{dt} &= Mn_{\text{tot}} \int d\mathbf{r} \mathbf{v}_{\text{mass}} \cdot \frac{\partial \mathbf{v}_{\text{mass}}}{\partial t} \\ &= -2\hbar n_{\text{tot}} \Gamma \int d\mathbf{r} \left(\frac{\partial \phi}{\partial t} \right)^2. \end{aligned} \quad (28)$$

Suppose that a vortex keeps its shape when it moves in the x direction at speed u : $\alpha(\mathbf{r}) = f(x - ut, y)$ and $\phi(\mathbf{r}) = g(x - ut, y)$, where f and g are functions expressing their profiles. Then, $(\partial\alpha/\partial t)^2 = u^2(\partial\alpha/\partial x)^2$ and $(\partial\phi/\partial t)^2 = u^2(\partial\phi/\partial x)^2$. Similarly, for a vortex moving in the y direction, $(\partial\alpha/\partial t)^2 = u^2(\partial\alpha/\partial y)^2$ and $(\partial\phi/\partial t)^2 = u^2(\partial\phi/\partial y)^2$. The averages of them result in

$$\left(\frac{\partial \alpha}{\partial t} \right)^2 = \frac{u^2}{2} (\nabla \alpha)^2, \quad \left(\frac{\partial \phi}{\partial t} \right)^2 = \frac{u^2}{2} (\nabla \phi)^2. \quad (29)$$

Combining Eqs. (25) and (28) and using Eq. (29), we estimate the energy dissipation as

$$\begin{aligned} \frac{dE}{dt} &= -\frac{\hbar n_{\text{tot}}}{\Gamma} \int d\mathbf{r} \left[(1 + \Gamma^2) \left(\frac{\partial \alpha}{\partial t} \right)^2 + 2\Gamma^2 \left(\frac{\partial \phi}{\partial t} \right)^2 \right] \\ &= -\frac{2M}{\hbar \Gamma} C \mathcal{N}_{\text{fric}} \log \left(\frac{R}{R_c} \right) u^2. \end{aligned} \quad (30)$$

Here,

$$\mathcal{N}_{\text{fric}} = (1 + \Gamma^2) \mathcal{N}_1 - \sigma_\phi^2, \quad (31)$$

where we used $\alpha = \sigma_\alpha \varphi$. The friction force is estimated by comparing Eqs. (15) and (30):

$$F_{\text{fric}} = \frac{2M}{\hbar \Gamma} C \mathcal{N}_{\text{fric}} \log \left(\frac{R}{R_c} \right) u. \quad (32)$$

In order to investigate the growth of characteristic domain size ξ , we apply the discussion of the coarsening dynamics in the 2D XY model [1, 8, 9, 11], where we expect $\xi \sim R \sim D$ and $u = d\xi/dt$. Equating the characteristic force between a vortex pair $F_{\text{pair}} \propto \mathcal{N}_2/\xi$ with the characteristic friction force $F_{\text{fric}} \propto (\mathcal{N}_{\text{fric}}/\Gamma) \log(\xi/R_c) d\xi/dt$, and rearranging terms, we have

$$\xi \log \left(\frac{\xi}{R_c} \right) \frac{d\xi}{dt} = A, \quad (33)$$

where A is a constant that depends on the dissipation rate and the characteristics of vortices as $A \propto -\Gamma \mathcal{N}_2 / \mathcal{N}_{\text{fric}}$. Integrating of Eq. (33) gives

$$\xi^2 \left[\log \left(\frac{\xi}{R_c} \right) - \frac{1}{2} \right] = 2A(t - t_0), \quad (34)$$

where t_0 is an integration constant. Employing the vortex density $\rho = 1/\xi^2$ and the maximum vortex density $\rho_c = 1/R_c^2$, we rewrite Eq. (34) as

$$t - t_0 = \frac{1}{4A} \frac{\log(\rho_c/\rho) - 1}{\rho}. \quad (35)$$

The number of vortices in ferromagnetic BECs is expected to yield Eq. (35), which is the same as the growth law for the XY model [9]. The difference between the XY model and ferromagnetic BECs is contained in factor A , which includes the information about vortices ($\mathcal{N}_{\text{fric}}$ and \mathcal{N}_2). Actually, the hydrodynamic equation with $\mathbf{v}_{\text{mass}} = 0$ corresponds to the XY model when $\hat{f}_z \simeq 0$ (namely, in a positive- q case). If $\mathbf{v}_{\text{mass}} = 0$, we just drop the E_{flow} terms in the above discussion, and then obtain the same equation as Eq. (35), although the factor A is different from that of the above case.

III. NUMERICAL SIMULATIONS

We perform numerical simulations by means of the dissipative GP equation (16) and the hydrodynamic equation (18). The advantage of the hydrodynamic equation is that the superfluid velocity \mathbf{v}_{mass} can be eliminated easily in simulations, which enables us to investigate what effects the superfluid flow has on the coarsening dynamics. Note that MHVs introduced in Sec. II A have both mass flow and spin flow around their cores. However, if we take $\mathbf{v}_{\text{mass}} = 0$ in simulations, the degrees of freedom of mass flow are eliminated. Then, the hydrodynamic equation reduces to the equation of motion of magnetizations, and what we call MHV in the discussion below becomes merely a spin vortex around which only the spin current circulates. In such a case, the index σ_ϕ is meaningless, and there exists only one combination of a vortex-antivortex pair; $\sigma_\alpha = 1$ and -1 .

In the simulations, the mass of an atom is given by a typical value for a spin-1 ^{87}Rb atom: $M = 1.44 \times 10^{-25}$ kg. The total number density is taken as $n_{\text{tot}} = \sqrt{2\pi} d^2 n_{3\text{D}}$ with $n_{3\text{D}} = 2.3 \times 10^{14} \text{ cm}^{-3}$ and $d = 1 \mu\text{m}$. The quadratic Zeeman energy is set to be $q/h = 10$ Hz. The dissipation rate is given by a typical value $\Gamma = 0.03$. Especially in the GP simulation, the system is in quasi-two dimensions: The wave function in the normal direction to the 2D plane is approximated by a Gaussian with width d . Interaction parameters are taken as $c_0 n_{3\text{D}}/h = 1.3$ kHz and $c_1 n_{3\text{D}} = -59$ Hz. The value of c_1 that we take here is ten times larger than a typical value of a spin-1 ^{87}Rb atom, which prevents the production of PCVs.

Initial states are given by randomly located four kinds of MHVs. The number of vortices of each kind is equal. Open boundary conditions are imposed on $256 \mu\text{m} \times 256 \mu\text{m}$ systems. The total number of vortices at first are 256, which implies that the average distance between vortices is about $16 \mu\text{m}$. Snapshots of the transverse and longitudinal magnetizations, the vorticity of mass flow, and the

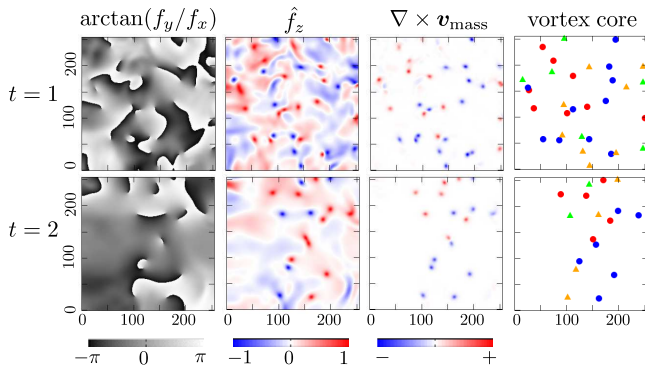


FIG. 2. (Color online) Snapshots of the transverse ($\arctan(f_y/f_x)$) and longitudinal (\hat{f}_z) magnetizations, the vorticity of mass flow ($\nabla \times \mathbf{v}_{\text{mass}}$), and the positions of vortex cores at time $t = 1$ s (top) and $t = 2$ s (bottom) are shown in the x - y plane, which are simulated by hydrodynamic simulations. The size of the snapshot is $256 \mu\text{m}$ on each side. The color of vortex core represents the directions of mass and spin flows ($\sigma_\phi = \pm 1, \sigma_\alpha = \pm 1$). Vortices that make annihilation pairs have the same symbol shape: red (+, +) and blue (-, -) circles, and green (+, -) and orange (-, +) triangles.

$(\sigma_\phi, \sigma_\alpha)$	\hat{f}_z	$\nabla \times \mathbf{v}_{\text{mass}}$
(+, +)	+	+
(-, -)	+	-
(+, -)	-	+
(-, +)	-	-

TABLE I. Signs of \hat{f}_z and $\nabla \times \mathbf{v}_{\text{mass}}$ at vortex cores with ($\sigma_\phi = \pm 1, \sigma_\alpha = \pm 1$).

positions of vortex cores are demonstrated in Fig. 2. The positions of vortex cores agree with those of maxima of $\nabla \times \mathbf{v}_{\text{mass}}$. The transverse magnetization and the vorticity of \mathbf{v}_{mass} are used to classify vortices into four kinds: $(\sigma_\phi, \sigma_\alpha) = (+, +), (-, -), (+, -)$ and $(-, +)$. The combination of σ_ϕ and σ_α is also related to the longitudinal magnetization at a vortex core, positive (negative) \hat{f}_z for $\sigma_\phi = \sigma_\alpha$ ($\sigma_\phi = -\sigma_\alpha$), as mentioned in Sec. II A. The sign of $\nabla \times \mathbf{v}_{\text{mass}}$ is related to the combination of σ_α and \hat{f}_z or simply σ_ϕ . Table I shows the signs of \hat{f}_z and $\nabla \times \mathbf{v}_{\text{mass}}$ at vortex cores for all the combinations of $(\sigma_\phi, \sigma_\alpha)$. The vortices with (+, +) and (-, -), which are represented as circles in Fig. 2, are a vortex-antivortex pair. Those with (+, -) and (-, +), which are represented as triangles, are another vortex-antivortex pair.

The number of vortices decreases with time as shown in Fig. 3(a). In the case of no superfluid flow, which is simulated by Eq. (18) with $\mathbf{v}_{\text{mass}} = 0$ at all times, the decay is slower than the other simulations. This suggests that the superfluid flow has an effect to accelerate the coarsening dynamics. However, the effect is not very simple, which is suggested in Fig. 3(b). The dashed line

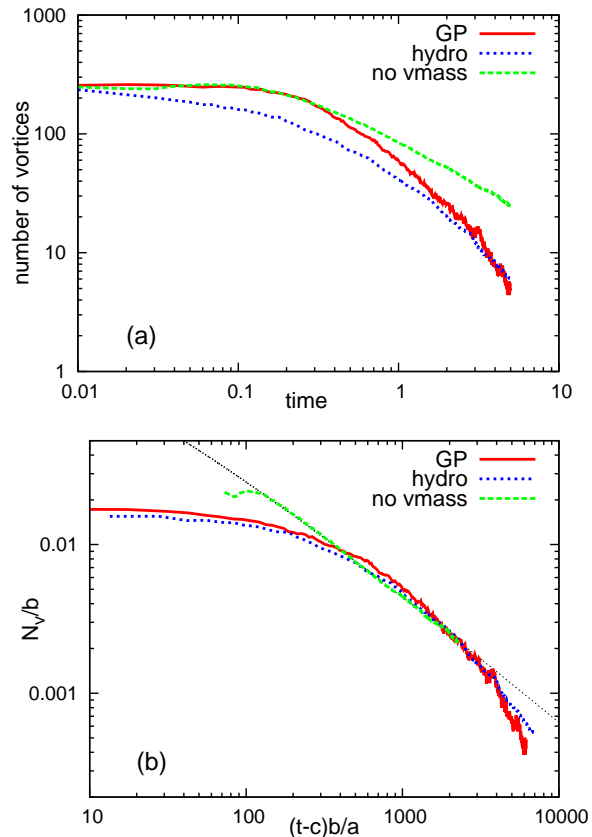


FIG. 3. (Color online) (a) Time dependence of the number of vortices simulated by GP equation (GP), hydrodynamic equation (hydro), and Eq. (18) in the absence of \mathbf{v}_{mass} (no vmass). Each curve is the average of ten simulations. (b) The same data replotted to show how they fit to $X = [\log(1/Y) - 1]/Y$ (dashed line) by means of the scaling Eq. (35).

represents the scaling, Eq. (35). The data are fitted to

$$t = a[\log(b/N_v) - 1]/N_v + c, \quad (36)$$

where t and N_v are time and the number of vortices, respectively. Note that $N_v = \rho L^2$, where L is the system size and $L = 256 \mu\text{m}$ in the simulations. For the fitting, the data in the range of $N_v \geq 20$ are used. The fitting parameters a and c correspond to $L^2/4A$ and t_0 , respectively. Parameter b , which corresponds to $\rho_c L^2$, is set to be a constant value, $b = (256/2.4)^2$. Actually, the core size is estimated to be $R_c \simeq 2.4 \mu\text{m}$ in the condensate of spin-1 ^{87}Rb atoms for $q/h = 10$ Hz. Since the fitting function is modified to be $(t - c)b/a = [\log(b/N_v) - 1](b/N_v)$, the data are plotted as $X = (t - c)b/a$ and $Y = N_v/b$, and they are expected to be on the curve $X = [\log(1/Y) - 1]/Y$. The values of fitting parameters in Fig. 3(b) are $(a, c) = (8.7, 0.24)$ in the GP simulation, $(8.1, 0.050)$ in the hydrodynamic simulation, and $(25.4, -0.16)$ in the absence of \mathbf{v}_{mass} . Although the data in the absence of \mathbf{v}_{mass} fit to the curve well, those of GP and hydrodynamic simulations are very different from the

expected scaling.

It might look strange that the curves of the GP and hydrodynamic simulations behave different in Fig. 3 (a), although they are similar in Fig. 3 (b). Actually, just the early-time dynamics is different between GP and hydrodynamic simulations. The given initial states, which are unstable, strongly affect the early-time dynamics. After the early time, both the GP and hydrodynamic simulations follow a common growth law. Since the growth law is not just a power law, the rescaled plots in Fig. 3 (b) behave similar even though they look different in the original plots.

The difference of situations between the GP and hydrodynamic simulations and the simulation without \mathbf{v}_{mass} is twofold. First, the superfluid flow may reduce friction (resistivity) in ferromagnetic BECs, which results in the faster decay of the number of vortices in the GP and hydrodynamic simulations than the simulation without \mathbf{v}_{mass} . Second, there is only one combination of vortex-antivortex pair in the absence of superfluid flow, which is the same situation in the XY model. In other words, when $\mathbf{v}_{\text{mass}} = 0$, σ_ϕ is meaningless, and vortices with the opposite signs of σ_α make a vortex-antivortex pair. By contrast, there are two combinations of vortex-antivortex pairs [i.e., one is $(\sigma_\phi, \sigma_\alpha) = (+, +)$ and $(-, -)$, and the other is $(+, -)$ and $(-, +)$] in the GP and hydrodynamic simulations.

In order to clarify the reason why the data in the above GP and hydrodynamic simulations do not agree with the expected scaling, we demonstrate the simulations in special cases where MHVs are limited to two kinds that can make a vortex-antivortex pair. MHVs of $(\sigma_\phi, \sigma_\alpha) = (+, +)$ are pair-annihilated with those of $(-, -)$ but not with the other kinds, $(+, -)$ or $(-, +)$. If there are only MHVs of $(+, +)$ and $(-, -)$, there is only one combination of annihilation pairs, which is the same situation as the simulation in the absence of superfluid flow. Then, we can see pure effects of \mathbf{v}_{mass} on the coarsening dynamics. The simulations with MHVs of $(+, -)$ and $(-, +)$ also give the same situation. In Fig. 4(a), the number of vortices decays slightly faster than the hydrodynamic simulations, and thus, much faster than the simulation in the absence of \mathbf{v}_{mass} . This fact implies that the coarsening dynamics is accelerated by superfluid flow. On the other hand, Fig. 4(b) illustrates better fitting for the two-kind-vortex data (labeled by “pp+mm” and “pm+mp”) than the four-kind-vortex data (labeled by “hydro”). The values of fitting parameters in Fig. 4(b) are $(a, c) = (6.5, -0.030)$ for “pp+mm”, and $(6.2, -0.030)$ for “pm+mp”. This result indicates that the scaling that describes the time dependence of vortex density is different from the expected one, Eq (35), when there are several combinations of vortex-antivortex pairs.

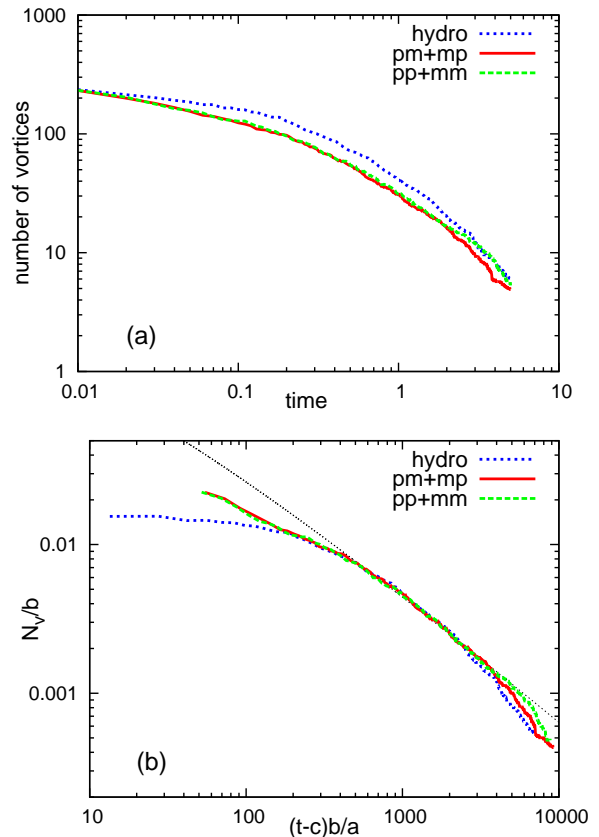


FIG. 4. (Color online) (a) Time dependence of the number of vortices simulated by hydrodynamic equations in the case where there are only two kinds of vortices, $(\sigma_\phi, \sigma_\alpha) = (+, +)$, $(-, -)$ (labeled with “pp+mm”) or $(+, -)$, $(-, +)$ (labeled with “pm+mp”). They decay faster than the case where four kinds of vortices exist, whose label is “hydro” (the same data in Fig. 3 (a)). Each curve is the average of 10 simulations. (b) The same data replotted to show how they fit to $X = (\log(1/Y) - 1)/Y$ (dashed line) by means of the scaling Eq. (35).

IV. REVISED GROWTH LAW

We here consider revising the scaling, and hence the growth law, for the case where there are two combinations (groups) of vortex-antivortex pairs. Vortices belonging to different groups cannot cause annihilation with each other. When the groups of vortex density ρ_1 and ρ_2 are mixed and coexist in the same space, we rewrite the total vortex density $\rho_{\text{tot}} = \rho_1 + \rho_2$ as

$$\rho_{\text{tot}} = 2\tilde{\rho} - 2\rho_0, \quad (37)$$

where $\tilde{\rho}$ represents a typical vortex density of a group and is supposed to obey the original scaling Eq. (35), and $2\rho_0$ corresponds to the difference between the expected and actual vortex densities. Suppose $\rho_1 = \tilde{\rho}$ and $\rho_2 = \tilde{\rho} - 2\rho_0$, where $\rho_0 > 0$. This implies that the vortices with density ρ_1 , which are in the majority, dominate the coarsening dynamics. The difference between them $\rho_1 - \rho_2 = 2\rho_0$

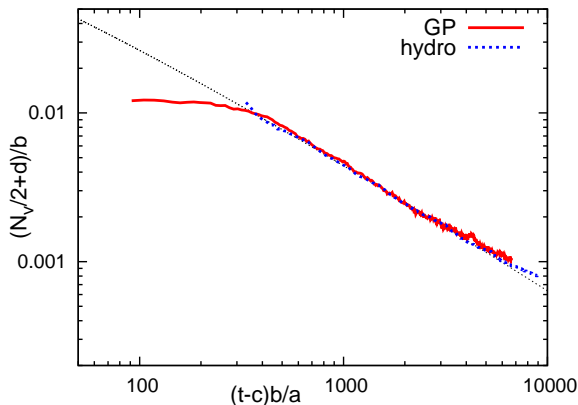


FIG. 5. (Color online) The same data of the GP and hydrodynamic simulations as Fig. 3 replotted to show how they fit to $X = (\log(1/Y) - 1)/Y$ (dashed line) by means of the revised scaling Eq. (38).

is almost independent of time, because the decay rate of vortex density is similar to each other if $\rho_1 \simeq \rho_2$. Even if $\rho_1 = \rho_2$ in the initial state, difference in vortex density often arises in a early time, when the vortex density is too high to obey the scaling. The difference is small, however, it is the key in the revised scaling.

Substituting $\tilde{\rho}$ of Eq. (37) into ρ of Eq. (35), we obtain a revised equation

$$t - t_0 = \frac{1}{4A} \frac{\log[\rho_c/(\rho_{\text{tot}}/2 + \rho_0)] - 1}{\rho_{\text{tot}}/2 + \rho_0}. \quad (38)$$

The same data of the GP and hydrodynamic simulations as that of Fig. 3, which are fitted to Eq. (38), are shown in Fig. 5. The data are actually fitted to

$$t = a\{\log[b/(N_v/2 + d)] - 1\}/(N_v/2 + d) + c \quad (39)$$

with $b = (256/2.4)^2$. The fitting parameters a and c correspond to $L^2/4A$ and t_0 , respectively, and d corresponds to $\rho_0 L^2$. Since the fitting function is modified to be $(t-c)b/a = \{\log[b/(N_v/2+d)] - 1\}[b/(N_v/2+d)]$, the data are plotted as $X = (t-c)b/a$ and $Y = (N_v/2+d)/b$, and they are expected to be on the curve $X = [\log(1/Y) - 1]/Y$. The values of fitting parameters in Fig. 5 are $(a, c, d) = (8.6, -0.059, 9.3)$ and $(6.4, -0.19, 6.0)$ in the GP and hydrodynamic simulations, respectively. The data are in good agreement with the revised scaling.

V. DISCUSSIONS AND CONCLUSIONS

We here discuss fitting parameters quantitatively. The the fitting parameter a , which corresponds to $L^2/4A \propto$

$\mathcal{N}_{\text{fric}}/\mathcal{N}_2$, is different between the presence and absence of superfluid flow. From Eqs. (11), (13), and (31), $\mathcal{N}_{\text{fric}}/\mathcal{N}_2 = -(1 + 3\Gamma^2)/6$ in the presence of superfluid flow. When there is no superfluid flow, $\mathcal{N}_{\text{fric}}/\mathcal{N}_2 = (1 + \Gamma^2)\mathcal{N}'_1/\mathcal{N}'_2$, where \mathcal{N}'_1 and \mathcal{N}'_2 are given by the same winding numbers as the 2D XY model, and thus, $\mathcal{N}'_1/\mathcal{N}'_2 = -1/2$. This means $\mathcal{N}_{\text{fric}}/\mathcal{N}_2 = -(1 + \Gamma^2)/2$ in the absence of superfluid flow. Thus, the value of a in the simulation in the absence of superfluid flow should be about three times larger than that in the GP and hydrodynamic simulations. Actually, in Fig. 3 (b), $a = 8.7$ and 8.1 for the GP and hydrodynamic simulations, respectively, and they are about 1/3 of $a = 25.4$ for the simulation in the absence of superfluid flow.

We have considered only MHVs in this paper. The coarsening dynamics becomes different and even faster in the cases of PCVs and one-component BECs than in the case of MHVs. Since some of the assumptions made in this paper are invalid for PCVs and one-component BECs, the growth laws in those cases should be different from that of the XY model or our revised one. We will present the study about those cases somewhere else.

In conclusion, the coarsening dynamics in ferromagnetic BECs with a positive quadratic Zeeman energy, in which magnetic anisotropy is similar to the XY model, leads to a different domain growth law from that of the XY model. We have proposed a revised growth law especially for the case where only MHVs exist. When several groups of vortex-antivortex pairs coexist in the same space, the difference in vortex densities of them leads to the revised growth law. In the absence of the superfluid flow, where there is only one combination of vortex-antivortex pairs, the growth law is the same as that of the XY model, and the coarsening dynamics is slower than in the presence of the flow. The effect of the superfluid flow is not only accelerating domain growth but also producing several combinations of vortex-antivortex pairs.

ACKNOWLEDGMENTS

This work was supported by MEXT KAKENHI (No. 26103514, “Fluctuation & Structure”) and JSPS KAKENHI (No. 22740265) of Japan. YK acknowledges the financial support from Inoue Foundation.

[1] A. J. Bray, *Adv. Phys.* **43**, 357 (1994).

[2] I. M. Lifshitz and V. V. Slyozov, *J. Phys. Chem. Solids*

- 19**, 35 (1961).
- [3] T. Ohta, D. Jasnow, and K. Kawasaki, Phys. Rev. Lett. **49**, 1223 (1982).
- [4] D. A. Huse, Phys. Rev. B **34**, 7845 (1986).
- [5] E. D. Siggia, Phys. Rev. A **20**, 595 (1979).
- [6] H. Furukawa, Phys. Rev. A **31**, 1103 (1985).
- [7] A. J. Bray, Phys. Rev. B **41**, 6724 (1990).
- [8] A. N. Pargellis, P. Finn, J. W. Goodby, P. Panizza, B. Yurke, and P. E. Cladis, Phys. Rev. A **46**, 7765 (1992).
- [9] B. Yurke, A. N. Pargellis, T. Kovacs, and D. A. Huse, Phys. Rev. E **47**, 1525 (1993).
- [10] S. Puri, A. J. Bray, and F. Rojas, Phys. Rev. E **52**, 4699 (1995).
- [11] A. D. Rutenberg and A. J. Bray, Phys. Rev. E **51**, 5499 (1995).
- [12] L. E. Sadler, J. M. Higbie, S. R. Leslie, M. Vengalattore, and D. M. Stamper-Kurn, Nature (London) **443**, 312 (2006).
- [13] M. Vengalattore, S. R. Leslie, J. Guzman, and D. M. Stamper-Kurn, Phys. Rev. Lett. **100**, 170403 (2008).
- [14] M. Vengalattore, J. Guzman, S. R. Leslie, F. Serwane, and D. M. Stamper-Kurn, Phys. Rev. A **81**, 053612 (2010).
- [15] S. De, D. L. Campbell, R. M. Price, A. Putra, B. M. Anderson, and I. B. Spielman, Phys. Rev. A **89**, 033631 (2014).
- [16] R. Barnett, D. Podolsky, and G. Refael, Phys. Rev. B **80**, 024420 (2009).
- [17] R. W. Cherng and E. Demler, Phys. Rev. A **83**, 053613 (2011); R. W. Cherng and E. Demler, Phys. Rev. A **83**, 053614 (2011).
- [18] K. Kudo and Y. Kawaguchi, Phys. Rev. A **84**, 043607 (2011).
- [19] K. Kudo and Y. Kawaguchi, Phys. Rev. A **88**, 013630 (2013).
- [20] K. Fujimoto and M. Tsubota, Phys. Rev. A **85**, 033642 (2012); Phys. Rev. A **85**, 053641 (2012).
- [21] M. Tsubota, Y. Aoki, and K. Fujimoto, Phys. Rev. A **88**, 061601(R) (2013).
- [22] K. Fujimoto and M. Tsubota, Phys. Rev. A **88**, 063628 (2013).
- [23] J. Hofmann, S. S. Natu, and S. Das Sarma, Phys. Rev. Lett. **113**, 095702 (2014).
- [24] J. Guzman, G.-B. Jo, A. N. Wenz, K. W. Murch, C. K. Thomas, and D. M. Stamper-Kurn, Phys. Rev. A **84**, 063625 (2011).
- [25] F. Gerbier, A. Widera, S. Fölling, O. Mandel, I. Bloch, Phys. Rev. A **73**, 041602(R) (2006).
- [26] K. Kudo and Y. Kawaguchi, Phys. Rev. A **82**, 053614 (2010).
- [27] K. Kawaguchi and M. Ueda, Phys. Rep. **520**, 253 (2012).
- [28] M. Tsubota, K. Kasamatsu, and M. Ueda, Phys. Rev. A **65**, 023603 (2002); K. Kasamatsu, M. Tsubota, and M. Ueda, Phys. Rev. A **67**, 033610 (2003).